Superdeformation in ^{68}Zn: Evidence for a New, Neutron-Rich Island of Superdeformation in $A \sim 70$ Nuclei

M. Devlin,[1] A. V. Afanasjev,[2,3,4] R. M. Clark,[5] D. R. LaFosse,[1,*] I. Y. Lee,[5] F. Lerma,[1] A. O. Macchiavelli,[5] R. W. MacLeod,[5] I. Ragnarsson,[2] P. Ring,[3] D. Rudolph,[6,†] D. G. Sarantites,[1] and P. G. Thirolf[6]

[1]*Chemistry Department, Washington University, St. Louis, Missouri 63130*

[2]*Department of Mathematical Physics, Lund Institute of Technology, Box 118, S-22100 Lund, Sweden*

[3]*Physik-Department, Technische Universität München, D-85747 Garching, Germany*

[4]*Nuclear Research Center, Latvian Academy of Sciences, LV-2169, Salaspils, Latvia*

[5]*Nuclear Science Division, E. O. Lawrence Berkeley National Laboratory, Berkeley, California 94720*

[6]*Sektion Physik, Ludwig-Maximilians-Universität München, D-85748 Garching, Germany*

(Received 19 January 1999)

A superdeformed rotational structure is reported in the stable nucleus ^{68}Zn. It has a transition quadrupole moment (Q_t) of $2.5^{+0.7}_{-0.4}$ e b ($\beta_2 \approx 0.4$), as measured by the residual Doppler shift method. Theoretical calculations suggest that two different configurations are possible candidates for this band. One is built without $h_{11/2}$ neutrons, as seen in superdeformed bands in the $A \sim 60$ region, while the other involves one $h_{11/2}$ neutron in analogy with superdeformed bands in the $A \sim 80$ region. The second of these candidate configurations is preferred, thus establishing a new, neutron-rich (relative to the line of β stability) region of superdeformation with $Z \sim 30$ and $N \sim 38$. [S0031-9007(99)09472-7]

PACS numbers: 21.10.Re, 21.10.Ky, 23.20.Lv, 27.50.+e

Superdeformed (SD) nuclei are known to exist in distinct regions, for which the neutron and proton numbers are near the magic numbers at superdeformation. All of the known SD regions are neutron deficient, relative to stable isotopes, even though such SD shell gaps exist throughout the Segrè chart. The reason for this situation is obvious: SD states are populated only at high spin, and to date only in fusion reactions. Given the experimental constraint that only stable beams and targets are available, the possible combinations leading to fusion are typically more neutron deficient than stable isotopes.

In medium mass nuclei ($40 < A < 100$), superdeformed bands have been identified in both the $A \sim 80$ [1,2] and $A \sim 60$ [3] regions. The numerous known SD bands in the $A \sim 80$ region are understood to involve neutron $h_{11/2}$ and proton $h_{11/2}$ (for $Z > 38$) excitations, associated with the deformed shell gaps at particle numbers 38 through 44 (see, for example, Refs. [4,5]). The important subject of the proton excitation involved in highly deformed and SD shapes at $Z = 38$ is currently in question [6,7]. In the $A \sim 60$ region, SD bands have been reported in isotopes of zinc: ^{60}Zn [8], ^{61}Zn [9], and ^{62}Zn [3]. These bands are understood to be multiple excitations of $\pi f_{7/2}$ and $\nu f_{7/2}$ particles into $\pi g_{9/2}$ and $\nu g_{9/2}$ intruder orbitals near the $Z = N = 30$ superdeformed shell gaps [10]. Other highly deformed bands have been reported in ^{63}Zn [11] and ^{65}Zn [9], with a similar origin. It is expected that SD structures also exist in the region $Z \sim 30$ and $N \gtrsim 38$, since in such a region the occupation of the $\pi g_{9/2}$ intruder orbitals seen in the $A \sim 60$ SD region could couple to the occupation of the $\nu h_{11/2}$ intruder orbitals seen in the $A \sim 80$ SD region.

We report here the first evidence for these types of SD states in the stable nucleus $^{68}_{30}Zn_{38}$. The reaction ^{48}Ca + ^{26}Mg (530 $\mu g/cm^2$) at 157 MeV beam energy was used to populate ^{68}Zn via the $\alpha 2n$ evaporation channel. The beam was accelerated by the 88" Cyclotron at Lawrence Berkeley National Laboratory. Gammasphere [12] with 95 Ge detectors was used to detect γ rays, in conjunction with the Microball [13], a 4π, 95-element CsI detector array which detected and identified evaporated light charged particles. Events with at least three cleanly detected γ rays were recorded for off-line analysis. Approximately 80% of the fusion yield involved only neutron evaporation. Less than 10% of the yield was contained in the 1α-gated data, representing $\approx 25 \times 10^6$ events. Of these, the $\alpha 2n$ channel, ^{68}Zn, is dominant; small amounts of ^{66,67}Zn are also observed.

Figure 1 shows the band observed in ^{68}Zn, and the coincident, low-spin transitions in ^{68}Zn which establish the assignment. The band consists of transitions at 1506, 1717, 1918, 2121, 2331, 2555, 2795, and possibly 3073 keV, and accounts for $\approx 1.9\%$ of the intensity of the $2^+ \rightarrow 0^+$ transition; the first six of these lines have γ-ray angular distributions consistent with quadrupole transitions, while the others have insufficient statistics to make such an assessment. No discrete linking transitions out of the band were identified. The decay of this band into normal-deformed structures proceeds primarily through a number of transitions observed at lower energy, as shown in Fig. 1, including one at 1508 keV, a doublet with the lowest energy band member. Most of the high-spin levels observed here have not been previously reported, and these data will be discussed in an upcoming

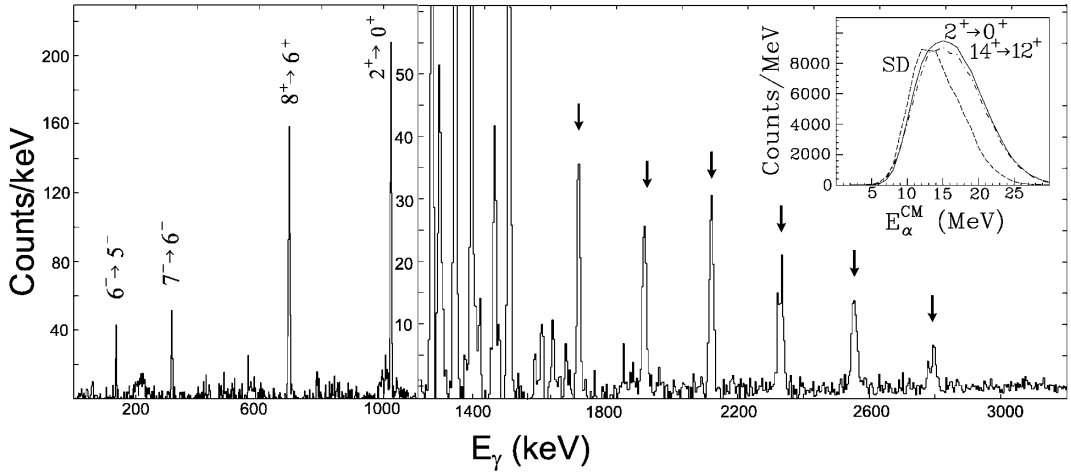

FIG. 1. The observed SD band in ^{68}Zn, obtained by double gating on all the transitions marked by arrows. The lines at lower energy are transitions in ^{68}Zn involved in the decay of the band. The inset shows the E_α spectrum in coincidence with the SD band (dashedline), the $2^+ \rightarrow 0^+$ transition (solid line), and the $14^+ \rightarrow 12^+$ transition (dot-dashed line).

publication [14]. Based on the observed feeding into known levels, the spin of the lowest SD level (I_0) is estimated as $(17 \pm 2)\hbar$; this estimate assumes two units of angular momentum between the mean intensity exit point of the SD band and the mean entry point into the known level scheme.

The dynamic moment of inertia $\mathcal{J}^{(2)}$ of the observed band is consistent with that of a superdeformed configuration, as can be seen in Fig. 2(A). Another typical feature of SD bands is that they are fed at high spin. The entry spin and excitation energy can be measured using the total γ-ray multiplicity and the excitation energy (E^*) obtained from the energies of all the emitted particles. Further, any subset of the evaporated particles contains similar information as E^*, though with reduced accuracy [15]. The inset of Fig. 1 shows the measured E_α distributions in coincidence with low-spin states in ^{68}Zn (solid line), ground-band states above 14^+ (dot-dashed line), and the observed SD band (dashed line). It can be seen that the SD band is populated at an average E_α lower than the average population of the ground band, and lower than that of the 14^+ state of the ground band. This implies that the SD band is populated at the highest E^*, and hence the highest spins obtained in residual ^{68}Zn nuclei in this reaction. Again, this is consistent with the population of an SD band.

Lifetimes of the states in the SD band were measured using the Doppler shift attenuation technique [16], in which the slowing of the recoil ion in the thin target is used as a clock to determine the γ-decay lifetimes of the fastest transitions. Figure 3 shows the resulting fractional Doppler shift $F(\tau)$ $(= \beta/\beta_0)$ for transitions in the SD band, as well as for some nonshifted, normal deformed transitions. Fits are made to the $F(\tau)$ function in order to determine the transition quadrupole moment (Q_t), using the model described in Refs. [16,17]. Side feeding is included based on the measured intensity pattern, and the side feeding times are assumed to be less than those of the preceding in-band transitions. The best fit gives $Q_t = 2.5^{+0.7}_{-0.4}$ e b (solid line), and is shown in Fig. 3.

In order to interpret this SD structure, detailed theoretical calculations have been carried out using the cranked relativistic mean field theory (CRMF) [18,19] and the (configuration-dependent) cranked Nilsson-Strutinsky (CNS) approach [20]. CRMF calculations in the SD minimum have been performed using the NLSH force [21]. Apart from the crossing frequencies, similar results were obtained with the NL3 [22] and NL1 [23] forces. In the CNS calculations, the standard set of the parameters for the Nilsson potential [20] has been used. The pairing correlations were not taken into account in the present calculations so the results can be considered realistic only at high spin ($I \geq 15\hbar$). The resulting configurations are labeled by $[p_1 p_2, n_1 n_2 n_3]$, where $p_1(n_1)$ is the number of proton (neutron) $f_{7/2}$ holes, $p_2(n_2)$ is the number of proton (neutron) $g_{9/2}$ particles, and n_3 is the number of $h_{11/2}$ neutrons (label n_3 is omitted if zero).

In the CNS calculations, the yrast line up to $I \sim 25\hbar$ is dominated by terminating bands. Then, the $[22, 04]$ configuration becomes yrast and at spins starting from $I \sim 30\hbar$ all yrast configurations include one $h_{11/2}$ neutron. The comparison of CNS and CRMF calculations with experiment reveals two likely configurations for the observed SD band, namely, $[22, 04]$ and $[22, 041]$. In the former, all single-particle orbitals below the $Z = 30$ and $N = 38$ SD shell gaps are filled [10]. The latter is built from the $[22, 04]$ configuration by the excitation of one neutron from the $\mathcal{N} = 3$ orbital into the lowest $h_{11/2}$ orbital. This excitation is shown by an arrow in Fig. 4 (bottom). This figure suggests that another favored configuration $[22, 031]$ is formed if the neutron is excited from the fourth $\mathcal{N} = 4$ orbital to the lowest $h_{11/2}$ orbital. In the calculations this configuration is comparable in energy to the $[22, 041]$

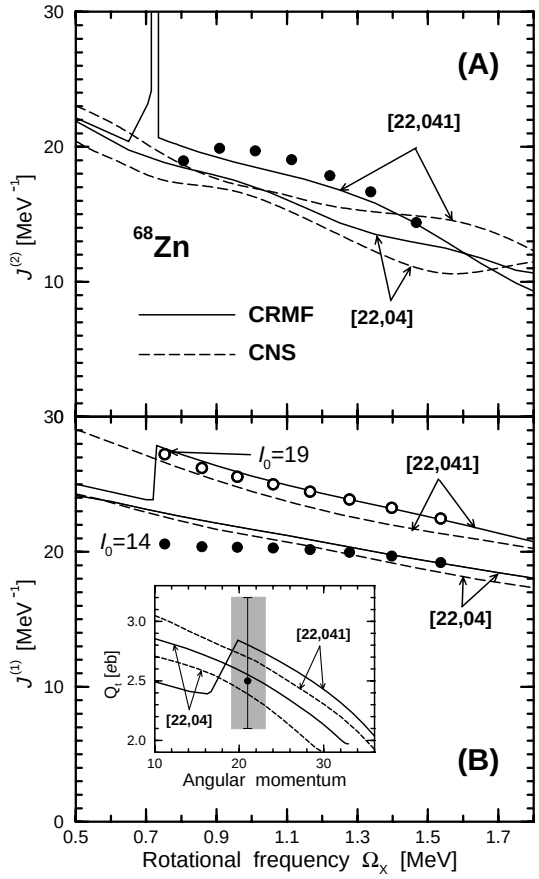

FIG. 2. Dynamic (A) and kinematic (B) moments of inertia of the observed SD band (circles), compared to the predicted properties of the expected configurations (lines, see text). The inset shows the Q_t values as a function of spin, as calculated in CRMF theory and the CNS approach. The shaded region approximately indicates the experimentally allowed region.

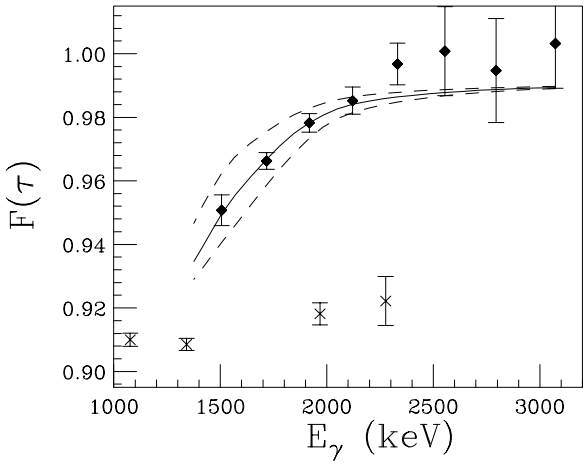

FIG. 3. Experimental fractional Doppler shifts $[F(\tau)]$ of the observed SD band (diamonds). The solid line represents $Q_t = 2.5\ e\,\mathrm{b}$, and the dashed lines correspond to the quoted uncertainties (which includes the uncertainty in I_0). The "×" symbols represent slower transitions (including the $2^+ \rightarrow 0^+$ and $4^+ \rightarrow 2^+$ transitions) which occur outside the target.

configuration. However, the calculated $\mathcal{J}^{(2)}$ moment of inertia and the effective alignment i_{eff} relative to the known highly deformed band in ^{58}Cu [24] for this configuration deviate considerably from experiment, and therefore the $[22, 031]$ configuration will not be considered in our further discussion.

Figure 2(A)compares the dynamic moments of inertia $\mathcal{J}^{(2)}$ of the $[22, 04]$ and $[22, 041]$ configurations to that of the observed band. In both model calculations, the best agreement is obtained for the $[22, 041]$ configuration. Indeed, in the CRMF theory the experimental $\mathcal{J}^{(2)}$ values are reproduced quite well over the whole frequency range. The jump in $\mathcal{J}^{(2)}$ calculated in CRMF at $\Omega_x \sim 0.83$ MeV for this configuration originates from the crossing between the $(r = +i)$ signatures of the lowest $\nu h_{11/2}$ and $\nu[301]3/2$ orbitals, as illustrated in Fig. 4 (bottom). This crossing does not appear in the CNS calculations since the main oscillator quantum number in the rotating potential $\mathcal{N}_{\mathrm{rot}}$ is treated as a preserved quantum number.

The top of Fig. 4 shows the effective alignments i_{eff} of the band in ^{68}Zn to the band observed in ^{58}Cu [24]. The best agreement is again obtained in CRMF calculations for the $[22, 041]$ configuration. The highly deformed band in ^{58}Cu has been chosen as a reference band since it is not effected strongly by pairing correlations and has a well-defined configuration [24,10]. Effective alignments relative to the high-spin part (above the crossing) of the SD band in ^{60}Zn leads to similar conclusions while the configuration of the SD band in ^{62}Zn is too uncertain [10] to add anything to this comparison. From the analysis of effective alignments two values of I_0 have been obtained. If the configuration $[22, 041]$ should be assigned to the observed band, then $I_0 = 19$. For the case of the $[22, 04]$ configuration, $I_0 = 14$ is the best value. With these configuration and spin assignments, calculated and experimental kinematic moments of inertia agree reasonably well, as seen in Fig. 2(B).

The inset of Fig. 2 shows the calculated Q_t for the two configurations of interest. The calculated values of Q_t averaged over the observed spin range are close to the experimental Q_t value. As shown in Table I and the inset of Fig. 2, both theoretical approaches predict a significant drop of collectivity in these configurations, a feature typical of SD bands in this mass region [10].

The experimental spin assignment, the comparison between calculated and experimental dynamic and kinematic moments of inertia, and the effective alignments favor the $[22, 041]$ configuration. In addition, this configuration is calculated to be 0.5–1.0 MeV lower in energy than the $[22, 04]$ configuration in the feeding region $(I \sim 35\hbar)$, depending on the model and parametrization. However, a definitive choice between these two configurations for the observed band is not possible at present, due in part to the similarity of the predicted properties of these configurations.

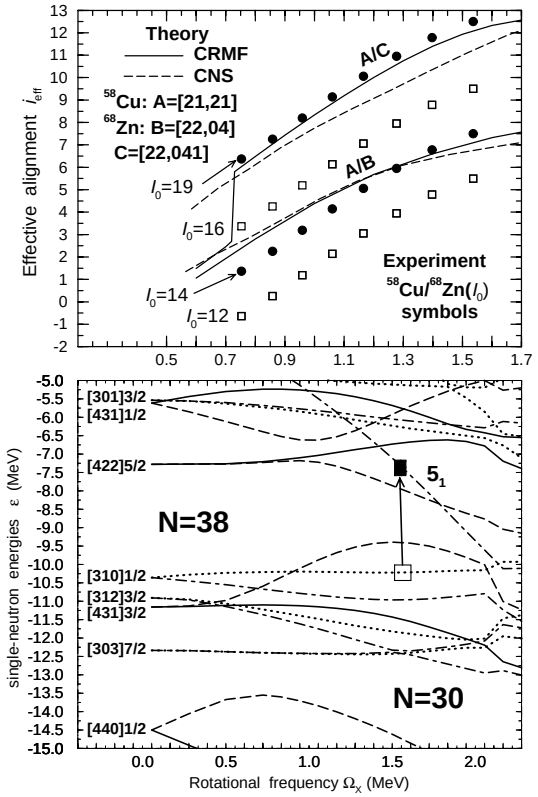

FIG. 4. (Bottom) Neutron single-particle energies (Routhians) given as a function of the rotational frequency Ω_x, as calculated along the deformation path of the $[22,04]$ configuration in ^{68}Zn in CRMF theory. Solid, dashed, dot-dashed, and dotted lines indicate $(\pi = +, r = -i)$, $(+,+i)$, $(-,+i)$, and $(-,-i)$ orbitals, respectively. The excitation leading to $[22,041]$ is indicated by the arrow. (Top) Effective alignments of the observed SD band, relative to the known highly deformed $[21,21]$ band in ^{58}Cu [24], for various choices of I_0. The lowest transition in ^{58}Cu is assigned as $11^+ \rightarrow 9^+$ 10. The effective alignment between two bands is the difference between their spins at constant rotational frequency.

In $A \sim 80$ superdeformed nuclei, the population of $h_{11/2}$ intruder orbitals for particle numbers 38–44 is responsible for the SD shapes. By analogy, the nuclei with $Z \sim 30$ and $N \sim 38$–44 should have SD bands built on $\nu h_{11/2}$ excitations as well, defining a new, neutron-rich island of superdeformation. This expectation is confirmed in the CRMF and CNS calculations, which predict the $[22,041]$ configuration to be yrast or close to yrast at high spin in ^{68}Zn. The SD band reported here in ^{68}Zn is most likely such an excitation, though as discussed the evidence for a $\nu h_{11/2}$ configuration is not definitive. Searches for SD structures in nearby, more neutron-rich nuclei would help resolve this issue and provide a more detailed understanding of this "neutron-rich" island of superdeformation.

This work is supported in part by the U.S. D.O.E. under Grant No. DE-FG02-88ER-40406 (WU), by the Swedish Natural Science Research Council, and by the German BMBF under projects No. 06 TM 875 and No. 06 LM 868. A. V. A. acknowledges support from the Alexander von Humboldt Foundation.

TABLE 1. Calculated deformation parameters for the two configurations discussed in the text, in both CRMF and CNS approaches [25]. Ranges listed are from $I_0 = 14, 19$ to $I = 30, 35$, for $[22,04]$ and $[22,041]$, respectively.

	CRMF		CNS	
Conf.	β_2	γ	β_2	γ
$[22,04]$	0.43–0.36	0°–5°	0.41–0.35	1°–7°
$[22,041]$	0.48–0.41	4°–10°	0.45–0.43	10°–20°

*Current address: Department of Physics and Astronomy, SUNY at Stony Brook, Stony Brook, NY 11794.
†Current address: Division of Cosmic and Subatomic Physics, Lund University, S-22100 Lund, Sweden.

[1] C. Baktash *et al.*, Phys. Rev. Lett. **74**, 1946 (1995).
[2] D. R. LaFosse *et al.*, Phys. Lett. B **354**, 34 (1995).
[3] C. Svensson *et al.*, Phys. Rev. Lett. **79**, 1233 (1997).
[4] W. Nazarewicz *et al.*, Nucl. Phys. **A435**, 397 (1985).
[5] J. Dudek *et al.*, Phys. Rev. C **35**, 1489 (1987).
[6] M. Devlin *et al.*, Phys. Lett. B **415**, 328 (1997).
[7] F. Lerma *et al.*, in *Proceedings of Nuclear Structure 98* (ORNL, Oak Ridge, TN, 1998), Vol. 1, p. 77; (to be published).
[8] C. Svensson *et al.*, Phys. Rev. Lett. **82**, 3400 (1999).
[9] C.-H. Yu *et al.*, in *Proceedings of Nuclear Structure 98* (Ref. [7]), Vol. 1, pp. 154, 155; (to be published).
[10] A. V. Afanasjev *et al.*, Phys. Rev. C (to be published).
[11] S. D. Paul *et al.*, in *Proceedings of Nuclear Structure 98* (Ref. [7]), Vol. 1, p. 100.
[12] I. Y. Lee, Nucl. Phys. **A520**, 641c (1990).
[13] D. G. Sarantites *et al.*, Nucl. Instrum. Methods Phys. Res., Sect. A **381**, 418 (1996).
[14] M. Devlin *et al.* (to be published).
[15] M. Devlin *et al.*, in *Proceedings of the Conference on Nuclear Structure at the Limits* (Report No. ANL/PHY-97/1, 1997), p. 220.
[16] B. Cederwall *et al.*, Nucl. Instrum. Methods Phy. Res., Sect. A **354**, 591 (1995).
[17] H.-Q. Jin *et al.*, Phys. Rev. Lett. **75**, 1471 (1995).
[18] A. V. Afanasjev *et al.*, Nucl. Phys. **A608**, 107 (1996).
[19] A. V. Afanasjev *et al.*, Nucl. Phys. **A634**, 395 (1998).
[20] T. Bengtsson and I. Ragnarsson, Nucl. Phys. **A436**, 14 (1985).
[21] M. M. Sharma *et al.*, Phys. Lett. B **312**, 377 (1993).
[22] G. A. Lalazissis *et al.*, Phys. Rev. C **55**, 540 (1997).
[23] P.-G. Reinhard *et al.*, Z. Phys. A **323**, 13 (1986).
[24] D. Rudolph *et al.*, Phys. Rev. Lett. **80**, 3018 (1998).
[25] Note that the β_2 and γ parameters describe the deformation of the potential in CNS approach and of the density distribution in the CRMF theory.